Title

A CALCULATION OF THE PHYSICAL CHARACTERISTICS OF NEGATIVE PION BEAMSuENERGY-LOSS DISTRIBUTION AND BRAGG CURVES

Authors

Curtis, Stanley B.
Raju, Mudundi R.

Publication Date

1967-06-05

UCRL-17606

cy.2

University of California

Ernest O. Lawrence Radiation Laboratory

A CALCULATION OF THE PHYSICAL CHARACTERISTICS OF NEGATIVE PION BEAMS-- ENERGY-LOSS DISTRIBUTION AND BRAGG CURVES

Stanley B. Curtis and Mudundi R. Raju

June 5, 1967

Berkeley, California

DISCLAIMER

Submitted to Radiation Res.

UCRL-17606
Preprint

UNIVERSITY OF CALIFORNIA

Lawrence Radiation Laboratory
Berkeley, California

AEC Contract No. W-7405-eng-48

A CALCULATION OF THE PHYSICAL CHARACTERISTICS OF NEGATIVE PION BEAMS-- ENERGY-LOSS DISTRIBUTION AND BRAGG CURVES

Stanley B. Curtis and Mudundi R. Raju

June 5, 1967

A CALCULATION OF THE PHYSICAL CHARACTERISTICS OF NEGATIVE PION BEAMS-- ENERGY-LOSS DISTRIBUTION AND BRAGG CURVES*

Stanley B. Curtis and Mudundi R. Raju

Lawrence Radiation Laboratory
University of California, Berkeley, California
and
Southwest Center for Advanced Studies, Dallas, Texas

3 Copies submitted

28 Manuscript pages

8 Figures

1 Table

---

*This work was done under the auspices of the U. S. Atomic Energy Commission, American Cancer Society, and Office of Naval Research.

Running head: Physical Characteristics of π^- BEAMS

[or Characteristics of π^- Beams]

Send proofs to

Stanley B. Curtis
Bldg. 29, Rm. 213
Lawrence Radiation Laboratory
Berkeley, California 94720

A Calculation of the Physical Characteristics of Negative Pion Beams--Energy-Loss Distribution and Bragg Curves. Radiation Res. _____, pp. _____ - _____ (1967).

CURTIS, STANLEY B. and RAJU, MUDUNDI R.

Donner Laboratory and Lawrence Radiation Laboratory
University of California, Berkeley, California
and
Southwest Center for Advanced Studies, Dallas, Texas

ABSTRACT

Calculations have been made of the dE/dx distribution (LET spectrum) and central-axis depth-dose curves (Bragg Curves) of stopping negative pion beams in water. Such beams are of interest because of the large deposition of energy at depth in the stopping pion region relative to that deposited at the surface. Nuclear interactions occurring when the pions come to rest cause low-energy highly ionizing particles to be emitted as the capturing nucleus breaks up, thus increasing the dose deposited in the stopping-pion region. The calculations show that for beams similar to those presently available experimentally, peak depth-to-entrance ratios of 3.4 and 2.9 can be expected in water for pure and contaminated beams respectively with a width of around 3.5 cm. The contaminated beam was assumed to contain 65% pions, 10% muons, and 25% electrons. The pions in these beams have a range of 25 cm of water. Comparison with experimental results taken with a lithium-drifted silicon detector shows that this detector gives a reasonable picture of the relative doses in water, and so can be used to measure isodose distributions and Bragg curves in water phantoms.

KEY WORDS: Physical characteristics of charged particle beams, negative pions, LET spectra, Bragg curves.

Considerable interest has been shown in the past several years in the possibility of using a negative pion (π^- -meson) beam in radiotherapy (1-4). Negative pions have unique properties not shared by any of the radiations now used in radiotherapy. The pions travel through matter at low ionization levels and, when they come to rest, are captured by nuclei and undergo violent nuclear interactions, causing low-energy, highly ionizing particles to be emitted as the nuclei break up. The depth of pion penetration depends on the initial energy of the particle. Most of the particles in an incoming beam survive and come to rest at the end of their range; the rest either decay or undergo nuclear interaction in flight. When the negative pion comes to rest in water, it is captured by either a proton or oxygen nucleus, forming a π^- -mesic atom. If it is captured by a proton, the resulting neutral atom diffuses through the medium until an oxygen nucleus is encountered. The pion is then captured by the oxygen nucleus, since the resulting energy of the system is lower; that is, the pion can be more tightly bound. The pion cascades down through the energy levels in the π^- -mesic atom until it reaches the ground state. The overlap of the nucleus and pion is then such that the probability of a nuclear interaction is unity and the interaction occurs. All this happens in times short compared with the mean lifetime of the pion of 2.6×10^{-8} second. Some work (2, 5, 6) has been done on the identification of the particles emerging from these nuclear interactions, or "stars" as they are called in nuclear emulsion.

An attempt is made here to calculate a few of the physical characteristics of pion beams (both pure and contaminated with other

particles) which are of interest in evaluating the potentialities of such a beam for radiotherapy. It should be emphasized at the outset that the following calculation is only as good as the input experimental data and the subsequent assumptions and approximations allow it to be. The final test of the suitability of pion beams for radiotherapy will come from the laboratory, where controlled experiments can be conducted on biological systems and the resulting effects can be carefully measured.

Throughout the calculation, many of the geometrical and physical input data reflect experimental conditions in the meson cave of the 184-inch cyclotron at the Lawrence Radiation Laboratory, where much of the experimental work is being carried out (3, 4). One artificial assumption is made: The incident pion beam is initially parallel and uniformly distributed. This is difficult to achieve experimentally, but it is certainly possible to achieve a beam parallel enough and with great enough uniformity to allow the following analysis to be valid. As comparison with experimental results shows, the analysis predicts well the gross features of the variation of ionization with depth in water, and there is no reason to believe that the resulting distribution of dE/dx is not roughly correct also.

The input data of the differential energy spectra of particles emerging from a pion interaction at rest come from the fine experiments performed in water-impregnated emulsion by P. H. Fowler and his group at the University of Bristol (2). By a subtraction process, they obtained the spectra of the various particles: protons, α particles, ^{7}Li ions, and the heavy recoils (boron, carbon, and nitrogen) which result from the capture of a negative pion by an oxygen nucleus in water.

To simplify the calculation, all the heavy recoils are assumed here to be carbon nuclei. The pion rest-mass energy of 140 MeV is available for overcoming the binding energy in the nucleus and giving kinetic energy to the emitted particles.

THE dE/dx DISTRIBUTION

We first define a function, $F(\epsilon)$, which we call the dE/dx or energy-loss distribution (sometimes called the LET spectrum). $F(\epsilon)$ is defined so that

$$\int F(\epsilon)\,d(\log\epsilon) = \text{total energy deposited per unit mass at the point in question per incident pion / cm}^2. \quad (1)$$

Here ϵ is the collision or ionization energy loss per unit length, dE/dx. We use the differential of the logarithm of ϵ because of the wide range in dE/dx involved in this problem. It will be convenient to plot the distribution logarithmically in dE/dx, and so equal distances along the abscissa will have equal weights if $F(\epsilon)$ is defined as above. The integral we note is proportional to the dose deposited at the point. We assume that all the energy is deposited locally, i.e., δ-ray corrections are small.

From the standard manner in which doses are calculated from particle fluxes, we can form the equality $\frac{dJ}{dE}\,\epsilon\,dE = F(\epsilon)\,d(\log\epsilon)$, (2) where dJ/dE is the differential energy spectrum at the point, i.e., the number of particles per unit energy interval per unit area per incident fluence. From Eq. 2 we solve for $F(\epsilon)$, obtaining

$$F(\epsilon) = 2.303\,\frac{dJ}{dE}\,\epsilon^2/\frac{d\epsilon}{dE}. \quad (3)$$

For a given ϵ, we can easily calculate $d\epsilon/dE$, which is the slope of the dE/dx-vs-E curve (7). In the low-energy region, the work of

Northcliffe has been used (8). A more difficult task is the determination of dJ/dE at the point in question for the various particles emerging from the pion stars. This quantity is calculated for one particle type in Appendix I, and the result is given here:

$$\frac{dJ}{dE} = \frac{\rho(Z)}{\epsilon} \int_{E}^{E_{max}} \frac{dJ}{dE}_{0} \, dE_{0}, \tag{4}$$

where $\rho(Z)$ = density of stopping pions at a depth Z in the water per incident pion fluence,

ϵ = dE/dx of particle of energy E,

E_{max} = maximum energy of particles emitted from a star--the exact value of E_{max} is not important, since the spectrum drops off steeply as a function of energy,

$\frac{dJ}{dE}_{0}$ = differential energy spectrum per pion star for the particle type in question,

E_{0} = initial energy of particles emerging from the star.

Substituting Eq. 4 into 3, we have, for the energy loss distribution,

$$F(\epsilon) = \frac{2.303 \, \rho(Z) \, \epsilon}{d\epsilon/dE} \int_{E}^{E_{max}} \frac{dJ}{dE}_{0} \, dE_{0}. \tag{5}$$

Note that $\int_{E}^{E_{max}} \frac{dJ}{dE}_{0} \, dE_{0}$ is just the total number of particles with initial energy greater than E. The total $F(\epsilon)$ for the stars is the sum of the contributions from each particle type,

$$F(\epsilon)_{\substack{\text{total} \\ \text{star}}} = F(\epsilon)_{\text{proton}} + F_{\alpha}(\epsilon) + F_{^{7}\text{Li}}(\epsilon) + F_{^{12}\text{C}}(\epsilon). \tag{6}$$

CONTRIBUTIONS FROM OTHER PARTICLES IN THE BEAM

The presently available pion beams unfortunately contribute low dE/dx components to the ionization deposited in the star region. Those pions which have not yet stopped have dE/dx higher than minimum, but lower than the high dE/dx of the charged particles emitted in the star. This contribution is calculated as follows. It is necessary to know the momentum or energy spread of the beam in order to calculate how many pions at any point have not yet stopped. We have assumed an initial beam of mean momentum 190 MeV/c, with the particle momenta in a Gaussian distribution with standard deviation 5 MeV/c. These are values taken from our experimental beam at the 184-inch cyclotron. The energy-loss distribution is calculated from Eq. 3, with

$$\frac{dJ}{dE}\,\epsilon = \frac{dJ}{dp_0}\,\frac{dp_0}{dE_0}\,\epsilon_0 \exp(-Z/\lambda), \tag{7}$$

where λ = the pion interaction mean free path (= 68 cm, the "geometric" mean freepath, in this calculation)

$$\frac{dJ}{dp_0} = \frac{1}{\sigma(2\pi)^{\frac{1}{2}}} \exp\left[-\frac{1}{2}\left(\frac{p_0 - \bar{p}}{\sigma}\right)^2\right],$$

with $\bar{p}$ = the mean initial pion momentum,

p_0 = the initial pion momentum,

σ = the standard deviation,

E_0 = the initial pion energy,

Z = depth into the water,

and ϵ_0 = dE/dx of the pions of initial energy E_0.

The exponential factor in Eq. 7 takes care of those pions lost from the beam through nuclear interaction before reaching the stopping region.

We assume no dose contribution from these interactions. We also neglect pion decay occurring in the water.

Accompanying the pions in the beam are muons and electrons of the same momentum. The approximate percentages of the various components of our initial beam are 65% pions, 25% electrons, and 10% muons (3). The muons are products of those pions which decay before reaching the final momentum-selection device. Their contribution to the energy-loss distribution is calculated in the same way as the pion contribution, with the omission of the exponential factor, because muons do not undergo absorption via the nuclear interaction. The electrons arise mainly from high-energy neutral pions decaying into two γ rays with subsequent electron-positron pair formation in the target. The electrons were assumed to be minimum ionizing everywhere and to undergo a slight buildup because of electromagnetic shower production through the water. The electron dose was considered to increase linearly with depth and to reach 1.5 times the initial dose at 40 cm depth. For comparison, the peak region of the ionization curve for the stopping pions occurred at about 25 cm in our beam.

CONSTRUCTION OF THE BRAGG CURVE

The portion of this study dealing with the pion and muon contaminations lends itself to computer analysis, and a program was written for the CDC 6600 to calculate the energy-loss distributions for the pion and muon components as a function of water depth and then to integrate these to obtain the energy deposited per unit volume so that relative ionization depth-dose curves (Bragg curves) could be obtained. The contribution from the stars in the stopping region was included by multiplying the density of stars at the various points in the star region by a constant and adding it to the other contributions. This constant value, which is calculated to be 29 MeV, can be considered the intrinsic contribution of one star to the ionization deposited on the average in the medium. It is just

$$\frac{1}{\rho(Z)} \int_{-\infty}^{\infty} F(\epsilon)_{\text{total star}} \, d(\log\epsilon)$$

where $F(\epsilon)_{\text{total star}}$ is given in Eq. 6.

RESULTS

The dE/dx distribution at 25.5 cm of water arising from all the components--stars, pions, muons, and electrons--are added together and shown in Fig. 1. The contribution from each component is also indicated. The spikes from the various components at high dE/dx arise at the spot where $d\epsilon/dE$ goes through zero (see Eq. 3). It is seen from the figure that there is considerable contamination from low-dE/dx components. The area under the curve is proportional to the dose, and by integrating this function at several depths and normalizing the results to the dose at the entrance, a normalized central-axis

depth-dose curve can be constructed. This is shown in Fig. 2 for a beam consisting only of pions, and in Fig. 3 for the contaminated beam described above, consisting of 65% pions, 10% muons, and 25% electrons. Also indicated in Fig. 3 is the contribution from neutrons, which is seen to be small. The calculation of the neutron contribution is outlined in Appendix II.

MULTIPLE SCATTERING AND STRAGGLING CONSIDERATIONS

We have neglected both multiple scattering of the beam and range-straggling effects. The multiple scattering is negligible because the calculated Bragg curve is a central-axis curve and the width of the multiple scattering distribution is small compared with the radius of the beam cross section used in our experiments. The standard deviation of the projected multiple scattering distribution of a pencil beam of stopping pions can be approximated well (see multiple scattering treatment in Appendix II) by

$$\sigma_{ms} = 7.63 \times 10^{-2} \; R_0^{0.95}$$

$$= 1.65 \text{ cm in the stopping pion region } (R_0 = 25.5 \text{ cm}).$$

Since this is small compared with the half-width of our beam of 3.8 cm, the spreading of the beam is appreciable only near the edges, and our central-axis value is relatively unaffected by multiple scattering. The correction on the beam axis would be 4%, assuming a uniform incident beam.

The amount of straggling can be approximated by using the graph and table given in the American Institute of Physics Handbook (9). The percentage change in the range due to straggling is Gaussianly distributed and the fractional standard deviation is given by

$$\sigma_{ss}/R_0 = \left(\frac{102.2}{mc^2}\right)^{\frac{1}{2}} \quad f(E/mc^2),$$

where m is the pion mass. The function $f(E/mc^2)$ is given as a function of energy in the graph for iron in the Handbook, and interpolation to other elements can be made by using the accompanying table. For pions of energy 96 MeV, the result in water is

$$\sigma_s / R_0 = 0.024 \text{ or } \sigma_s = 0.6 \text{ cm.}$$

Figure 4 shows the density (as a function of depth) of stopping pions, as calculated by the computer program. The shape of the curve is due to the initial momentum spread. A Gaussian approximation with standard deviation 1.6 cm is shown as the solid curve. It is seen that the pions stop in an approximately Gaussian distribution. The folding of two Gaussians produces another Gaussian of standard deviation,

$$\sigma = (\sigma_1^2 + \sigma_2^2)^{\frac{1}{2}},$$

where σ_1 and σ_2 are the standard deviation of each Gaussian. Thus, folding the straggling distribution into the distribution due to the initial momentum spread yields the total standard deviation,

$$\sigma = 1.7 \text{ cm.}$$

We see that the straggling correction adds only 1 mm to the spread due to momentum spread of the initial beam. Therefore, it has been neglected in the calculation.

Finally, there is a small correction to the straggling due to multiple scattering. This effect has been estimated and is a small fraction of the straggling correction and so is also neglected.

DISCUSSION

It is seen from Figs. 2 and 3 that the dose in the stopping pion region is increased markedly by the presence of the particles produced in the nuclear interactions. For the pure pion beam, the maximum depth-to-entrance dose ratio is 3.4 and the full width at half maximum (i.e., the width of the curve when it has a value half way between 1.0 and its maximum value) is 3.5 cm. For the contaminated beam, the maximum dose ratio is 2.9 and the full width at half maximum is 4 cm. The maxima of both these curves occur at 25 cm of water for a beam of 190 MeV/c initial momentum.

It is possible to calculate the relative contributions to the dose from the various types of particles at, for instance, the maximum of the dose curve. The percentage of dose caused by the pions which have not yet stopped varies greatly through the peak region. Table I gives percentage contributions from the various particles at 25.5 cm of water, near the maximum of the dose curve, for both the pure and contaminated beams. Here, the pions which have not yet stopped contribute 35% and 30% of the dose, respectively. It is seen that the most heavily ionizing components (^{4}He, ^{7}Li, ^{12}C ions, and neutrons) account for 32% and 28% of the dose for the pure and contaminated beams, respectively. The other 30% of the dose comes from the protons, which are seen from Fig. 1 to be mostly in the low dE/dx range. These percentages vary as a function of incident particle momentum as well as momentum spread of the beam.

Although this calculation was carried out under the assumption that the medium in which the pions stopped was water, it is of some interest to compare these results with preliminary data of a dose

curve measured with a lithium-drifted silicon detector in the pion beam at the Berkeley 184-inch cyclotron, as reported by Raju et al (10). This comparison is shown in Fig. 5. Experimentally, the linearity of the electronic system required is difficult to achieve over the large range of pulse heights present in the stopping pion region, and the experimental data presented must be considered of a preliminary nature (10). The agreement is good, however, and could probably be made better by adjusting the momentum spread of the incident beam used in the calculation. Computer runs were made with spreads of 3, 5 and 7 MeV/c and the best fit (5 MeV/c) was chosen. This is a reasonable value and had been assumed prior to these experiments by the physics groups using this pion beam.

The higher dose, beyond the pion peak in the experimental data, has not been completely explained, but may well be due to the contribution from negative muon-capture processes in the silicon detector. The probability for such processes rises as Z^4, for low Z where Z is the atomic number of the stopping material. The probability for nuclear capture of the muon equals the probability for muon decay at $Z \simeq 10$. Since silicon has a Z of 14 and oxygen has a Z of 8, capture processes will dominate in the detector while decay will dominate in water. The capture process is $\mu^- + p \rightarrow n + \nu$. The neutrino carries off most of the energy. The most probable fate of the resulting excited nucleus is for one or more low-energy neutrons to be "boiled off" in an evaporation process. This would lead to a small increase in dose in the silicon detector around the muon stopping region. Another process, which occurs with less probability, is the direct emission of charged

particles. A theoretical calculation of this correction for silicon has not been attempted. The dose in the muon stopping region in water arising from muon-decay electrons has been estimated to be not more than 10% of the muon contribution shown in Fig. 3, and so was not included in the figure.

In view of the fact that the calculation was made for water and the experimental data were obtained in a silicon detector with a somewhat nonuniform pion beam, the comparison between the theoretical and experimental results as shown in Fig. 5 is considered satisfactory. In fact, the similarity between the two results indicates that the nuclear interactions occurring when pions are captured in silicon do not produce significantly different particle types and spectra from those occurring in water. Thus, silicon detectors appear to be useful dosimeters for measuring the distribution of dose from pion beams in water.

SUMMARY

The physical properties of a stopping negative pion beam have been studied in connection with dosimetry experiments with such beams at the Berkeley 184-inch cyclotron. Calculations have been made of the dE/dx distribution in the stopping pion region, and central-axis depth-dose curves (Bragg curves) have been computed with the assumption of a uniform parallel incident beam with a large enough cross section so that multiple scattering can be neglected. A Gaussianly distributed incident momentum spread is assumed such that the width of the Bragg peak in the stopping region due to momentum straggling is large compared with range straggling effects. This approximates well our experimental situation. Although the calculations were carried out with water as the stopping medium, comparison of the resulting Bragg curve with an experimental curve obtained with a silicon detector shows good agreement. This result implies that the nuclear products emerging from a silicon nucleus after pion capture do not alter significantly the dose in silicon from the dose expected in water. Thus it appears that silicon detectors can be used to obtain information on dose distributions of stopping pions beams in water phantoms.

ACKNOWLEDGMENTS

It is a pleasure to acknowledge the assistance of Mr. Michael Levitt, who was responsible for the numerical analysis of the neutron contribution presented in Appendix II, and Mr. John Sperinde, who helped with the considerations of multiple scattering effects. The suggestions and encouragement of Professor C. Richman are gratefully acknowledged. We wish also to acknowledge the support of Professors C. A. Tobias and J. H. Lawrence throughout the course of this work.

This work was performed under the auspices of the United States Atomic Energy Commission, the American Cancer Society, and the Office of Naval Research.

APPENDIX

I. Calculation of dJ/dE at depth Z in the Pion Stopping Region

We assume a uniformly distributed parallel beam of incident pions to calculate dJ/dE at a depth of water, Z, in the pion stopping region on the central axis of the beam. The beam is assumed to have a large enough cross section so that edge effects are nonexistent on the central axis. We let dJ/dE_0 be the number of particles of a given type (e.g., protons) of energy between E_0 and $E_0 + dE_0$ emitted isotropically from a pion interaction. The quantity dJ/dE_0 is the differential energy spectrum per star. The spectra measured by P. H. Fowler (2) in oxygen have been used in this calculation. Now we let $f_D(E_0, r)$ equal the number of particles of initial energy between E_0 and $E_0 + dE_0$ crossing a unit area at a distance r from a star. If we integrate this function over a sphere, we must account for all the particles between E_0 and $E_0 + dE_0$ emitted from the star.

Thus,

$$\int_{\text{sphere}} f_D(E_0, r)\ dA = \frac{dJ}{dE_0}, \tag{1A}$$

where $dA = r^2 \sin\theta\, d\theta\, d\phi$.

Since r is constant on the sphere, the integration is trivial and yields

$$4\pi r^2 f_D(E_0, r) = \frac{dJ}{dE_0}. \tag{2A}$$

Now to calculate the number of particles per unit area at Z with energy greater than E from sources (stars) in the vicinity, we must integrate $f_D(E_0, r)$ over energy from E up to E_{max} and over volume to include all those stars which will contribute particles of energy E or greater at the point. We integrate the function $f_D(E_0, r)\ \rho(Z, r)$, where

$f_D(E_0, r)$ is the number of particles crossing unit area per star at a distance r from the point and $\rho(Z, r)$ is the density of stars (i.e., number per unit volume) at a distance r from the point Z. We have

$$J(\geq E) = \int_E^{E_{max}} \int_0^{R(E_0)-R(E)} f_D(E_0, r)\, \rho(Z, r)\, dA\, dr\, dE_0. \tag{3A}$$

We now assume that the density of stars, ρ, varies linearly over the region where most of the energy from a star is deposited. That is, we make the approximation

$$\rho(Z, r) = \rho(Z) + K\, r \cos\theta, \tag{4A}$$

where $r \cos\theta$ is the distance along the z axis and $\rho(Z)$ is the density of stars at Z. Figure 6 shows to what extent this is a valid approximation for the pion beam we have used in our experiments to date. The density of stars is shown as a function of depth through the star region. The fraction of energy deposited by a star is shown as a function of distance from the star center, which is placed arbitrarily near the center of the star region. It is seen that within 6 mm, 80% of the star energy has been deposited. Over such a distance, the star density can be considered as varying linearly.

Substituting Eqs. 2A and 4A into 3A, and integrating over dA, we have

$$J(\geq E) = \rho(Z) \int_E^{E_{max}} \int_0^{R(E_0)-R(E)} \frac{dJ}{dE_0}\, dr\, dE_0. \tag{5A}$$

We note that the r^2 factors cancel. This is simply a result of the fact that although the flux through a unit area from a source falls as $1/r^2$, the number of sources on a spherical shell increases as r^2. Also, the term involving the linear variation of the density vanishes,

since

$$\int_0^{\pi} \cos\theta \sin\theta \, d\theta = 0.$$

The upper limit for r in Eq. 5A is explained in Fig. 7. R(E) denotes the range of a particle with energy E. For stars further than $R(E_0) - R(E)$ from the point of interest, the particle with initial energy E_0 could not reach the point with energy E or greater and so should not be included in $J(\geq E)$. This upper limit, then, corresponds to those particles which arrive at the point of interest with energy E.

Integration over dr yields

$$J(\geq E) = \rho(Z) \int_E^{Emax} [R(E_0) - R(E)] \frac{dJ}{dE_0} dE_0. \quad (6A)$$

The differential spectrum dJ/dE is obtained by differentiating Eq. 6A with respect to E, yielding, in absolute value,

$$\frac{dJ}{dE} = \frac{\rho(Z)}{\epsilon} \int_E^{Emax} \frac{dJ}{dE_0} dE_0. \quad (7A)$$

Here we have made use of the well-known relationship

$$\frac{d}{dx} \int_a^x f(y)\, dy = f(x),$$

and the fact that

$$\frac{dR(E)}{dE} = \frac{1}{\epsilon}.$$

II. Summary of the Technique for Estimating the Neutron Contribution in the Bragg Peak

The neutron differential energy spectrum from the pion-oxygen interactions was taken as the interpolated curve given in Fowler's paper (2). Depth-dose curves for wide parallel monoenergetic neutron beams with slab geometry were weighted according to the neutron spectrum to yield a depth-dose curve corresponding to the neutron spectrum from a pion star. That is,

$$D(r) = \int D(E_0, r) \frac{dJ_n}{dE_0} dE_0 \Big/ \int \frac{dJ_n}{dE_0} dE_0, \qquad (B1)$$

where $D(r)$ = the dose per neutron/cm^2 at a distance r,

$D(E_0, r)$ = the neutron dose per incident neutron/cm^2 of initial energy E_0 at a distance r,

$\frac{dJ_n}{dE_0}$ = the differential energy spectrum of neutrons from a star. $D(E_0, r)$ were obtained from the work of Snyder and Neufeld (11) and Zerby and Kinney (12). The above expression is for a parallel beam incident on a semi-infinite slab of tissue. Since the neutrons of interest here have rather high energies (average energy $\approx$ 23 MeV), we assume that a negligible number leave the slab in a direction opposite to the incident beam direction. We can then assume that from a point source (i.e., a pion star) the dose will fall off as $1/r^2$ times the above function $D(r)$, that is,

$$f(r) = \frac{3}{4\pi r^2} D(r) \text{ rads/star.} \qquad (B2)$$

Here $f(r)$ is the rads per star deposited by neutrons at a distance r from the star. The factor of three arises because three neutrons on

the average are emitted per star. The final expression for the central axis dose at point Z is given by

$$D(Z) = \frac{3}{4\pi} \int\int\int \rho(x, y, z) \frac{D(r)}{r^2} \, dxdydz, \qquad (B3)$$

where $\rho(x, y, z)$ is the density of stars, number per unit volume at the point (x, y, z), and r is the distance from the volume element to the dose point at Z. The variation of the density along z was assumed to be that shown in Fig. 4. The variations along x and y were chosen to be identical and symmetrical. The initial beam was assumed uniform and square in shape with a width of 8 cm. It was then assumed that the beam spread out due to multiple scattering. The points of arrest of the pions, and so the density of pions stars, were described in the stopping region by a simplified theory of multiple scattering where $(1/p\beta)^2$ can be written to a good approximation as $K R^{-k}$, where K and k are constants and R is the residual range of the pion [see the appendix of (1), for example]. We have used $K = 1.86 \times 10^{-3}$ and $k = 1.10$. The spread of one element of the beam is a Gaussian distribution in this case with a standard deviation 1.65 cm. Thus, an approximation of the three-dimensional distribution of pion stars could be constructed. The resultant density as well as the D(r) function were known only numerically; therefore, a numerical integration of Eq. B3 was performed. A computer program was developed for the CDC 6600 to perform the integration. The main feature of this program was a sliding interval size such that negligible error was introduced at small r, where $1/r^2$ is large.

Calculations were made every 2 cm through the star region except near the center, where values were computed every 1/3 cm. The results are shown in Fig. 8, and are also indicated on the Bragg curve in Fig. 2.

Table I. Percentage contribution of various particles to the dose at the maximum of the dose curve.

Particle type	Pure beam (no electrons or muons)	Contaminated beam (10% muons, 25% electrons in incident beam)
	Percent contribution	
Protons	33	28
He ions	14	12
^{7}Li ions	2	2
^{12}C ions	9	8
Neutrons	7	6
Pions (not yet stopped)	35	30
Electrons	—	10
Muons	—	4

Beam Conditions: 190±5 MeV/c - momentum beam in water

REFERENCES

1. P. H. FOWLER and D. H. PERKINS, The possibility of therapeutic applications of beams of negative π mesons. Nature 189, 524-528 (1961).
2. P. H. FOWLER, π Meson versus cancer? Proc. Phys. Soc. 85, 1051-1066 (1965).
3. C. RICHMAN, H. ACETO, M. R. RAJU, and B. SCHWARTZ, The radiotherapeutic possibilities of negative pions-preliminary physical experiments. Am. J. Roentgenol. Radium Therapy and Nucl. Med. 96, 777-790 (1966).
4. M. R. RAJU, H. ACETO, and C. RICHMAN, Pion studies with silicon detectors. Nucl. Instr. Methods 37, 152-158 (1965).
5. P. AMMIRAJU and L. M. LEDERMAN, A diffusion chamber study of very slow mesons. IV. Absorption of pions in light nuclei. Nuovo Cimento 4, 283-306 (1956).
6. M. G. K. MENON, H. MUIRHEAD, and O. ROCHAT, Nuclear reactions produced by slow negative π-mesons. Phil. Mag. 41, 583-618 (1950).
7. As found in W. H. BARKAS and M. J. BERGER, Tables of energy losses and ranges of heavy charged particles; in Studies in Penetration of Charged Particles in Matter, Natl. Acad. Sci.-Natl. Res. Council Publication 1133, 103-172 (1964).
8. L. C. NORTHCLIFFE, Passage of heavy ions through matter, Am. Rev. Nucl. Sci. 13, 67-102 (1963). Also found as Appendix B in publication referred to in Ref. 7 above, pages 353-388.

9. H. BICHSEL, Passage of charged particles through matter, in American Institute of Physics Handbook, McGraw-Hill, Second Edition, Section 8c, Page 8-37 (1963).

10. M. R. RAJU, E. J. LAMPO, S. B. CURTIS, J. M. SPERINDE and C. RICHMAN, Lithium-drifted silicon detector used as a pulse dosimeter, in the Proceedings of the 13th Nuclear Science Symposium on Instrumentation in Space and Laboratory, Boston, Massachusetts, Oct. 19-21, 1966, IEEE Trans. Nucl. Sci. NS 10 [1], 559 (1966).

11. W. S. SNYDER and J. NEUFELD, Calculated depth-dose curves in tissue for broad beams of fast neutrons. Brit. J. Radiol. 28, 342-350 (1955).

12. C. D. ZERBY and W. E. KINNEY, Calculated tissue current-to-dose conversion factors for nucleons below 400 MeV. USAEC Report ORNL-TM-1038, Oak Ridge National Laboratory, 1965.

FIGURE LEGENDS

Fig. 1. The dE/dx distribution of a contaminated negative pion beam at 25.5 cm of water in the Bragg peak region calculated for an incident Gaussianly distributed momentum distribution 190 ± 5 MeV/c. The contribution of each component is shown. The beam was assumed to be composed initially of 65% pions, 25% electrons, and 10% muons. The ordinate is in MeV per gram per logarithmic interval of dE/dx per incident pion/cm^2.

Fig. 2. A normalized central-axis depth-dose curve in water for a pure negative pion beam of incident momentum 190 ± 5 MeV/c. The additional contribution of dose in the peak region due to the pion interactions or stars is indicated.

Fig. 3. A normalized central-axis depth-dose curve in water for a contaminated beam of negative pions of incident momentum 190 ± 5 MeV/c. The contributions from the contaminant particles are indicated.

Fig. 4. The relative density of stopping pions of 190 ± 5 MeV/c in water as a function of depth through the stopping region. The points denote results from the computer program. The solid curve is a Gaussian fit with a standard deviation of 1.6 cm.

Fig. 5. Comparison of the calculated Bragg curve (Fig. 3) with experimental results obtained with a lithium-drifted silicon detector in a water phantom.

Fig. 6. The fraction of energy deposited by a single pion star inside a given distance plotted against distance from the star. The

variation of the density of stopping pions (star density) is plotted through the peak of the star region for comparison.

Fig. 7. Explanation of the upper limit of integration over r. R(E) denotes the range of a particle with energy E. The "point of interest" is the point where the dose is being calculated. Only those particles of initial energy E_0 which are emitted closer to the dose point than $R(E_0) - R(E)$ will reach it with energy greater than E.

Fig. 8. Neutron contribution to the dose as a function of depth in water for the negative pion beam described in the text. The dose is normalized to the incident contaminated beam dose and is also plotted in Fig. 2.

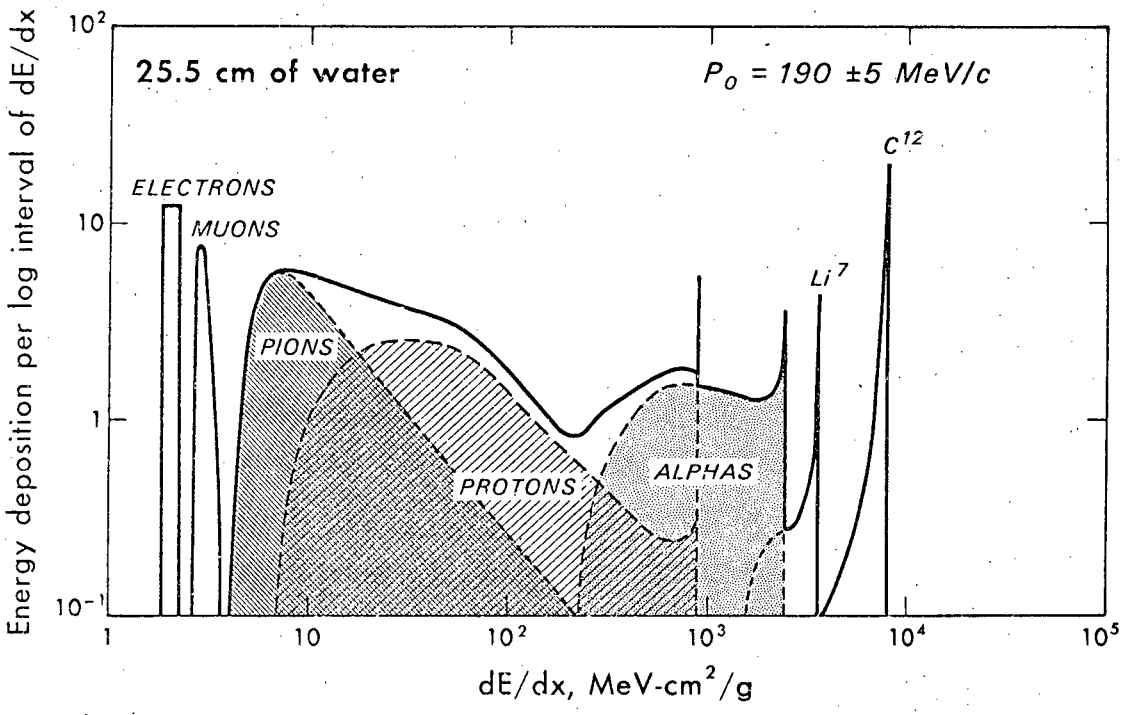

DBL 673-1581

Fig. 1.

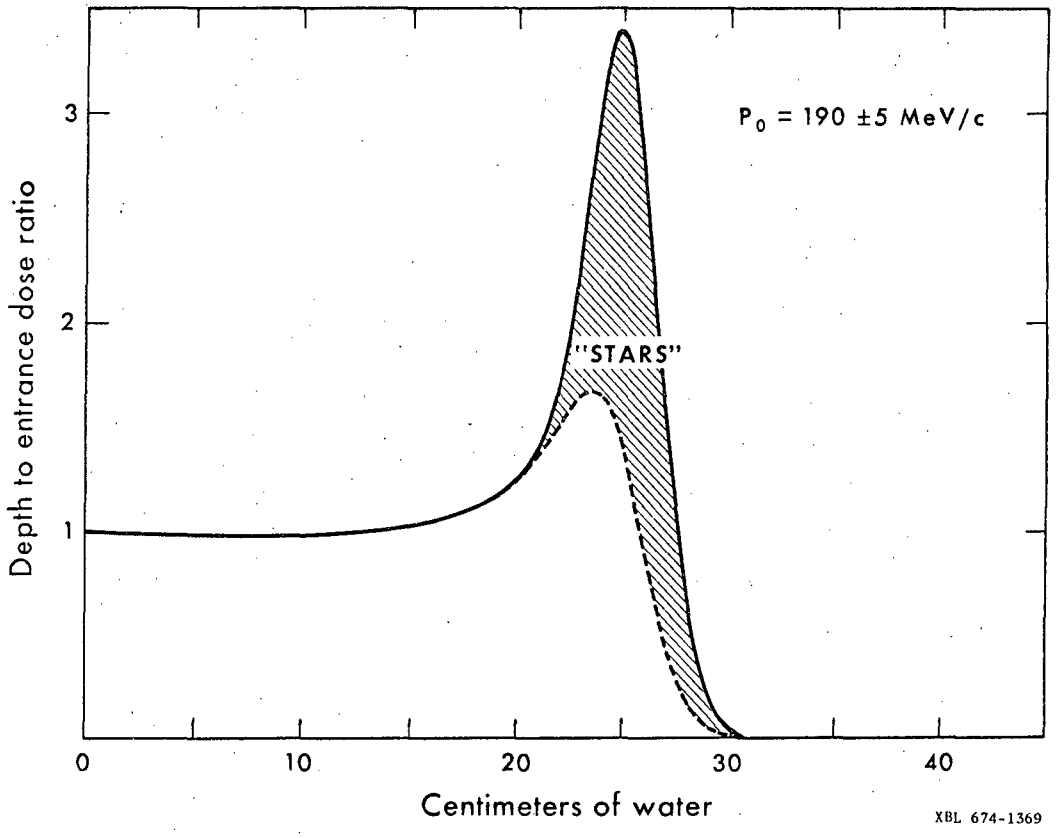
P_0 = 190 ±5 MeV/c
"STARS"
Depth to entrance dose ratio
Centimeters of water
0
10
20
30
40
1
2
3
XBL 674-1369

Fig. 2.

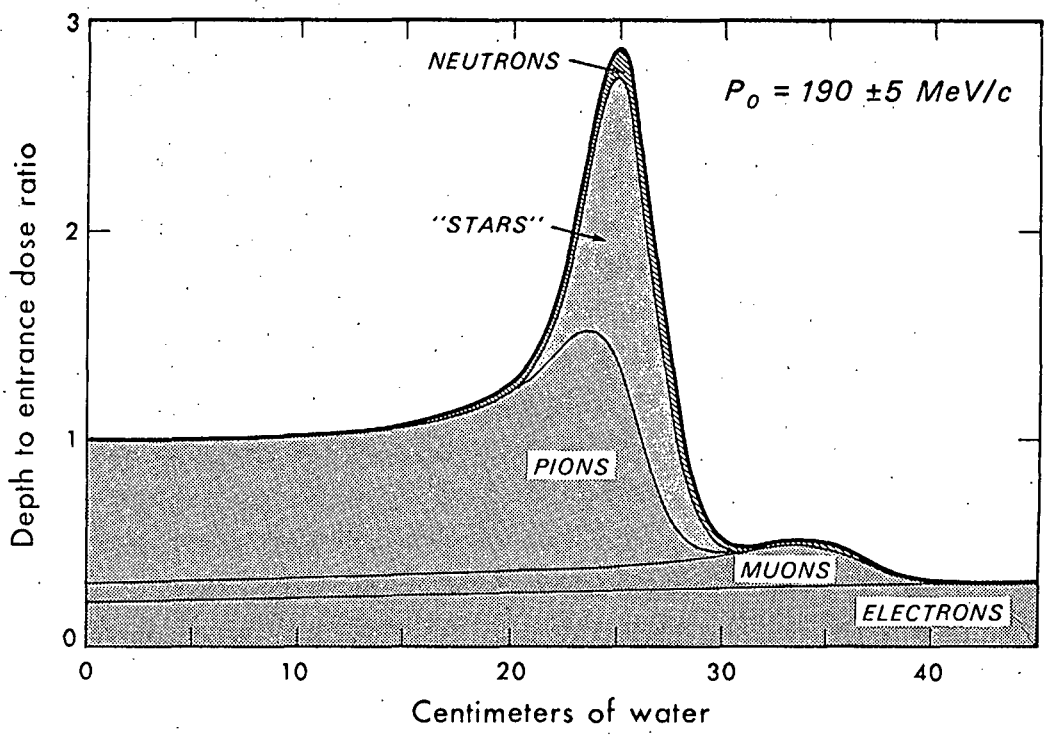
NEUTRONS
P_0 = 190 ±5 MeV/c
"STARS"
PIONS
MUONS
ELECTRONS
Depth to entrance dose ratio
Centimeters of water
0
1
2
3
0
10
20
30
40
DBL 673-1580

Fig. 3.

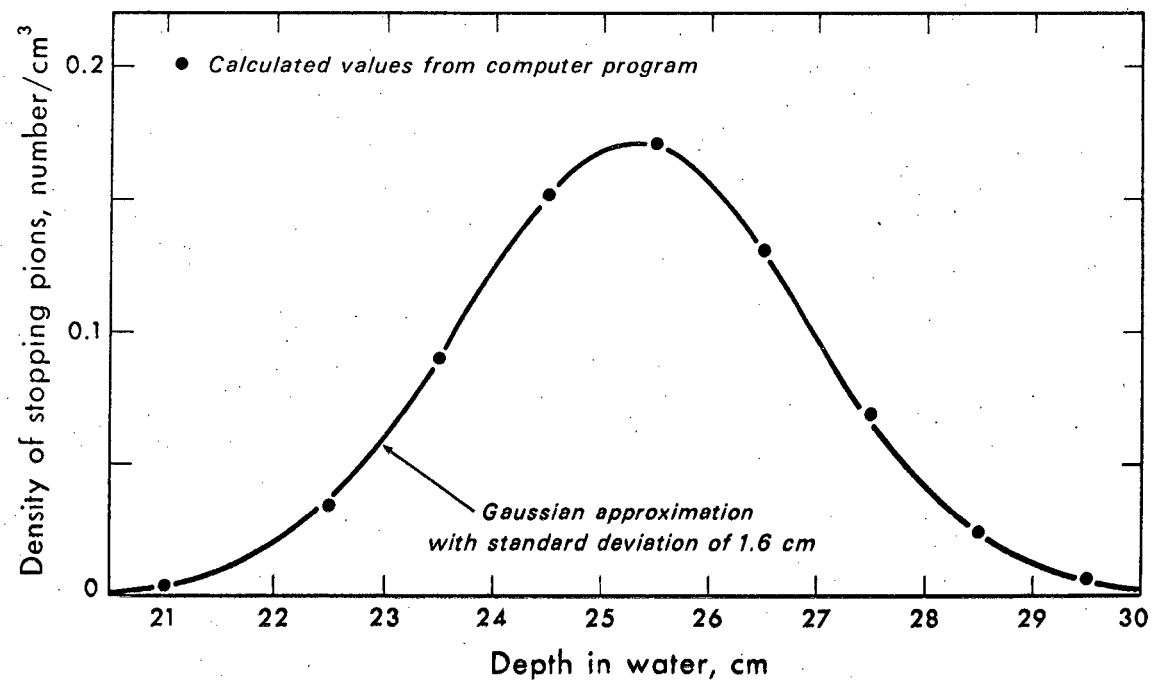

DBL 673-1583

Fig. 4.

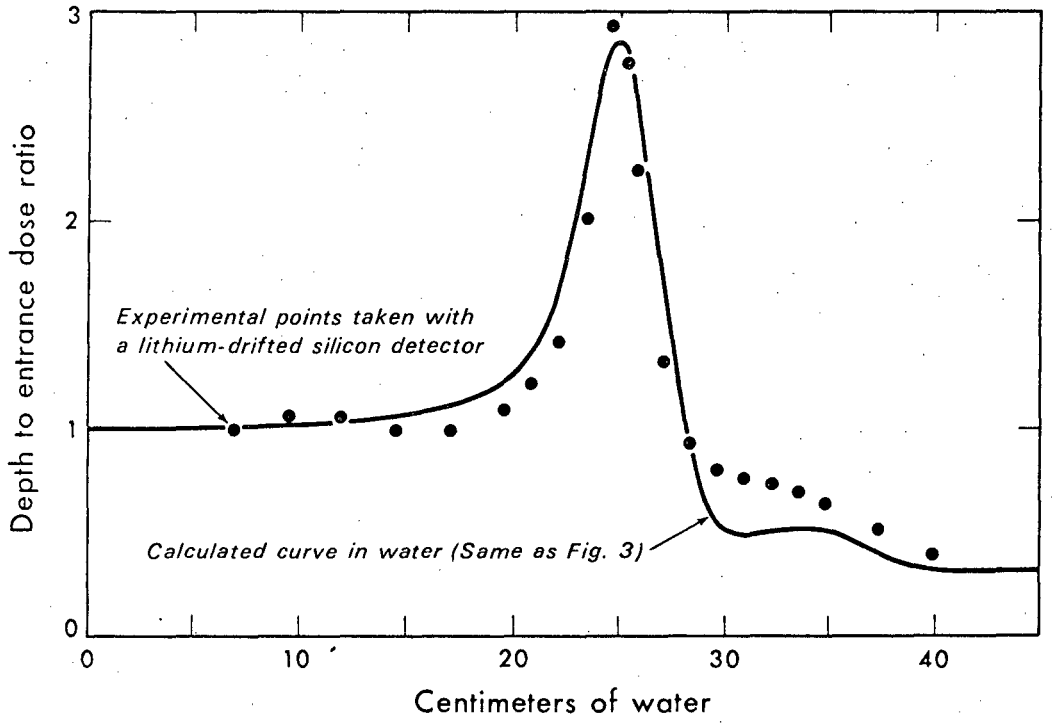

DBL 673-1582

Fig. 5.

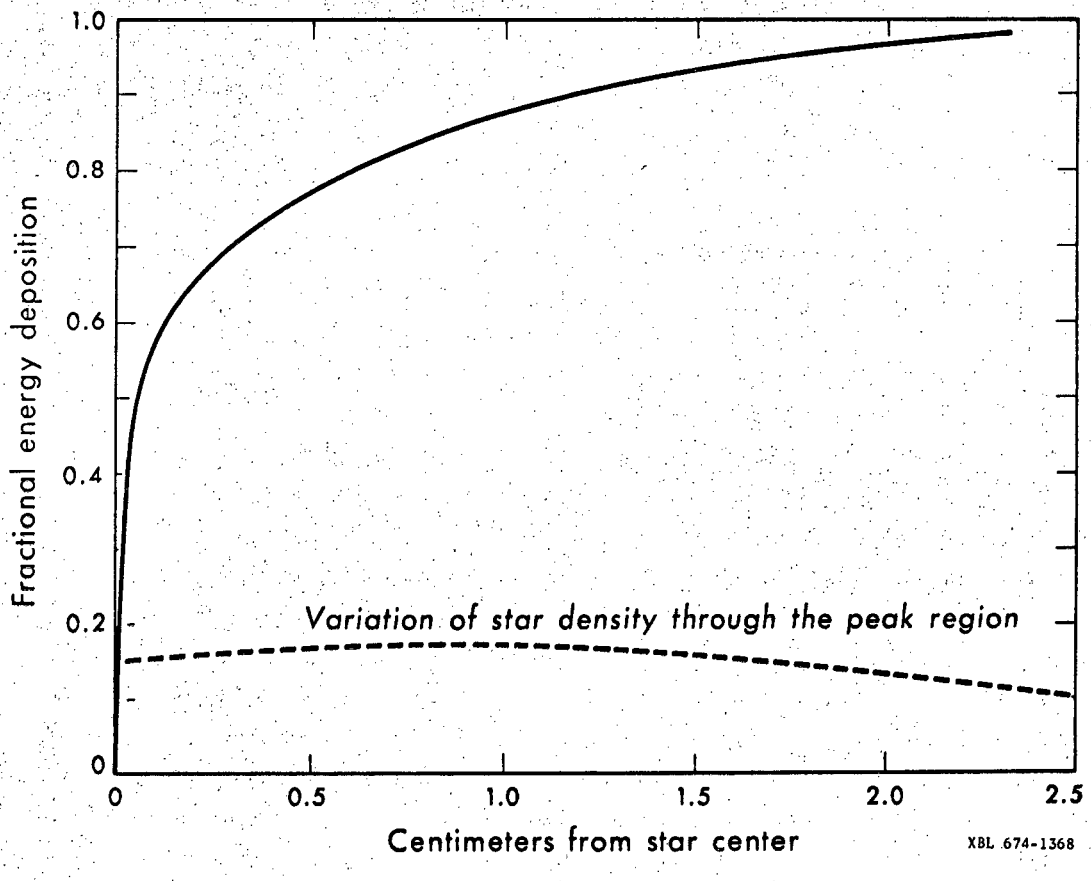
1.0
0.8
0.6
0.4
0.2
0
Fractional energy deposition
Variation of star density through the peak region
0
0.5
1.0
1.5
2.0
2.5
Centimeters from star center
XBL 674-1368

Fig. 6.

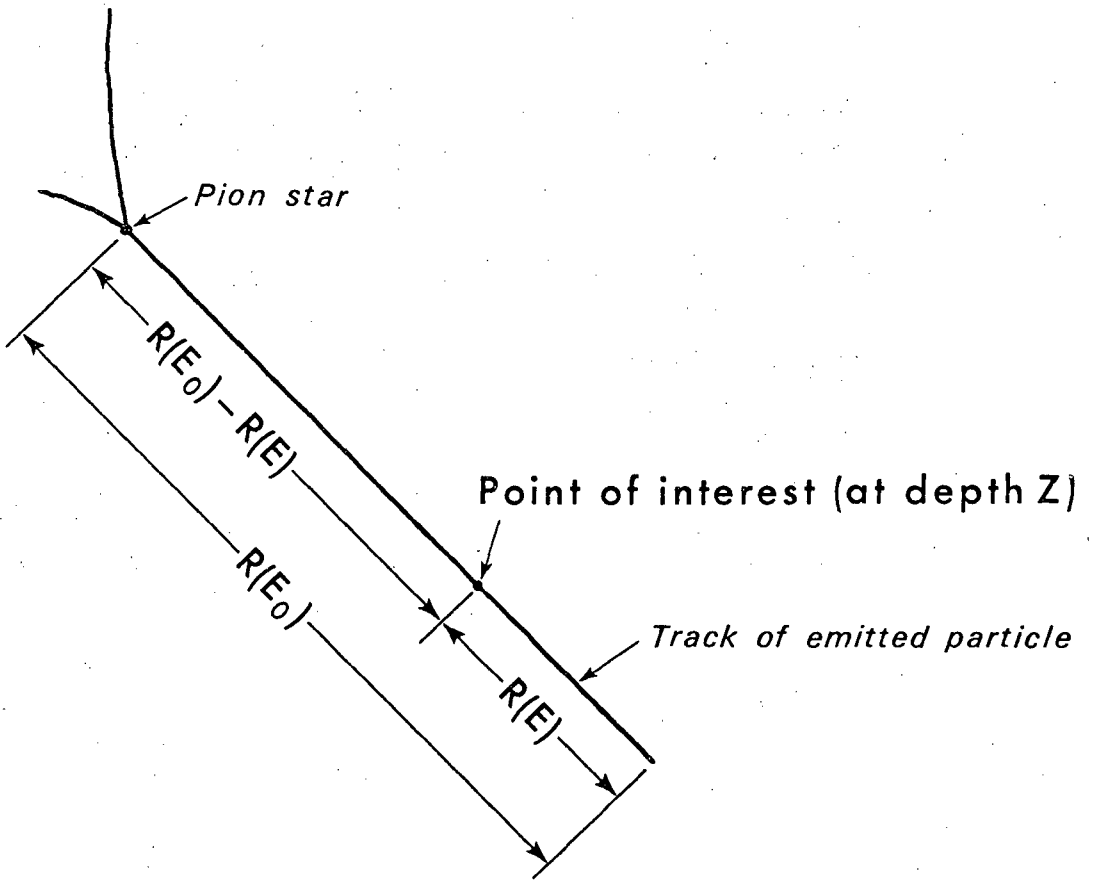

DBL 673-1585

Fig. 7.

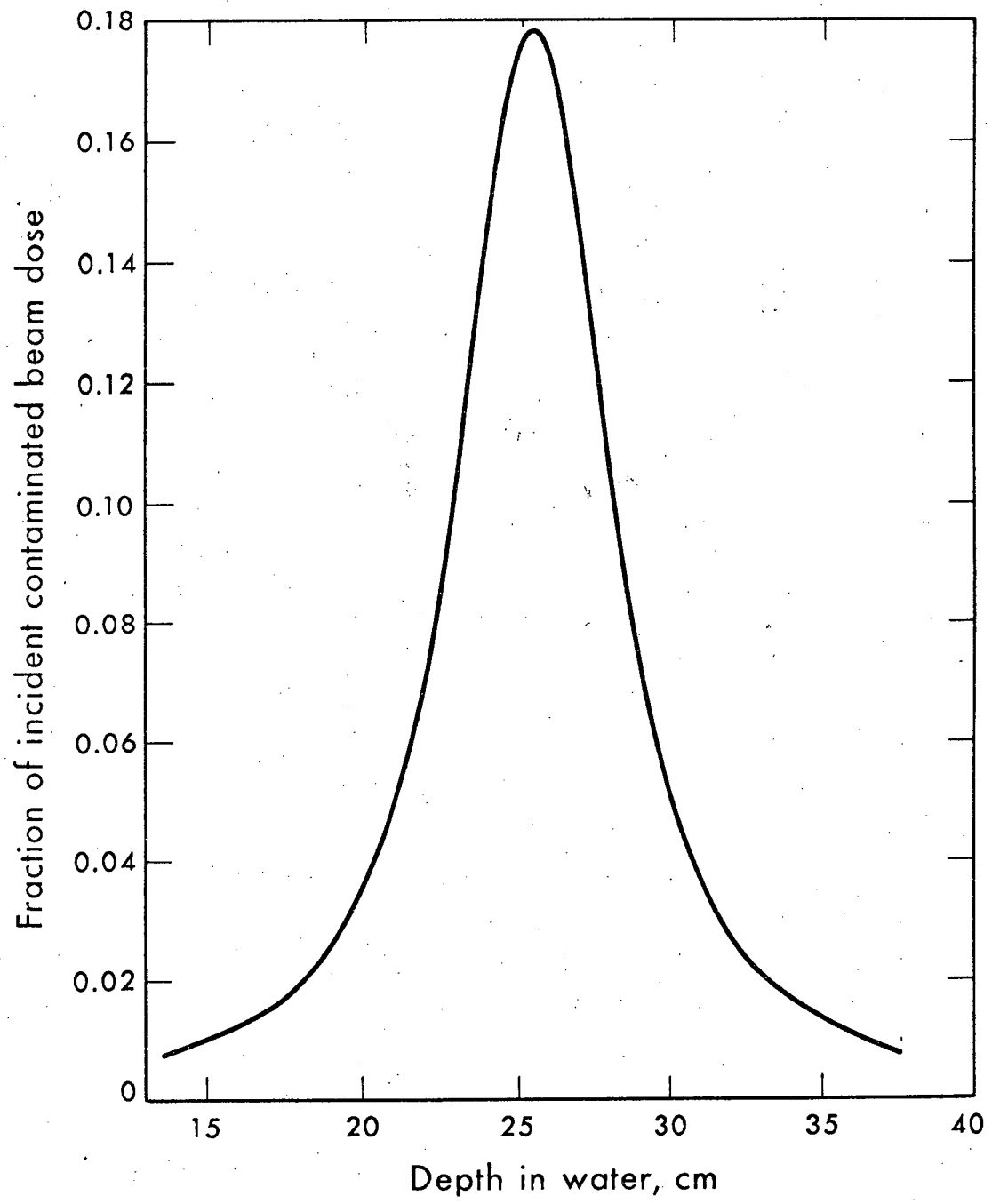
Fraction of incident contaminated beam dose
0.18
0.16
0.14
0.12
0.10
0.08
0.06
0.04
0.02
0
15
20
25
30
35
40
Depth in water, cm
DBL 673-1584

Fig. 8.